Malte Merk[1]
Fakultät für Maschinenwesen,
Technische Universität München,
Garching 85747, Germany
e-mail: merk@tfd.mw.tum.de

Camilo Silva
Fakultät für Maschinenwesen,
Technische Universität München,
Garching 85747, Germany

Wolfgang Polifke
Fakultät für Maschinenwesen,
Technische Universität München,
Garching 85747, Germany

Renaud Gaudron
Laboratoire EM2C, CNRS,
CentraleSupélec,
Université Paris Saclay,
3, rue Joliot Curie,
Gif-sur-Yvette cedex 91192, France

Marco Gatti
Laboratoire EM2C, CNRS,
CentraleSupélec,
Université Paris Saclay,
3, rue Joliot Curie,
Gif-sur-Yvette cedex 91192, France

Clément Mirat
Laboratoire EM2C, CNRS,
CentraleSupélec,
Université Paris Saclay,
3, rue Joliot Curie,
Gif-sur-Yvette cedex 91192, France

Thierry Schuller
Institut de Mécanique des
Fluides Toulouse (IMFT),
Université de Toulouse,
CNRS, INPT, UPS,
Toulouse 31062, France

Direct Assessment of the Acoustic Scattering Matrix of a Turbulent Swirl Combustor by Combining System Identification, Large Eddy Simulation and Analytical Approaches

This study assesses and compares two alternative approaches to determine the acoustic scattering matrix of a premixed turbulent swirl combustor: (1) The acoustic scattering matrix coefficients are obtained directly from a compressible large eddy simulation (LES). Specifically, the incoming and outgoing characteristic waves f *and* g *extracted from the LES are used to determine the respective transmission and reflection coefficients via System Identification (SI) techniques. (2) The flame transfer function (FTF) is identified from LES time series data of upstream velocity and heat release rate. The transfer matrix of the reactive combustor is then derived by combining the FTF with the Rankine–Hugoniot (RH) relations across a compact heat source and a transfer matrix of the cold combustor, which is deduced from a linear network model. Linear algebraic transformation of the transfer matrix consequently yields the combustor scattering matrix. In a cross-comparison study that includes comprehensive experimental data, it is shown that both approaches successfully predict the scattering matrix of the reactive turbulent swirl combustor.* [DOI: 10.1115/1.4040731]

Introduction

Increasing environmental awareness and stringent emission regulations drive gas turbine manufacturers toward lean combustion technology [1]. This technology comes with lower emissions of nitrogen oxides or unburnt hydrocarbons. Unfortunately, lean combustion systems are also susceptible to self-excited thermoacoustic instabilities, which may generate pressure fluctuations of intolerable amplitude, causing severe damage to an engine.

For thermoacoustic stability analysis, a combustion system may conveniently be regarded as an assembly of elements, see Fig. 1. The acoustic properties of individual combustor elements may be described in terms of the respective *transfer matrix* or alternatively the *scattering matrix*. Transfer and scattering matrices are interchangeable inasmuch as one may be transformed into the other by straightforward algebraic manipulation. However, as we shall elaborate below, these two descriptions of acoustic behavior are not fully equivalent to each other and there are situations where it is advantageous to use one instead of the other.

The idea of describing individual elements of a complex acoustic system by two-port matrices was introduced by Munjal [2]. This approach has the advantage that the transfer behavior is independent of upstream and downstream impedance, which would not be true for a one-port element. For simple element types such as duct sections or area jumps, matrix coefficients may be derived approximately by analytical methods. Coefficient values for the geometrically more complex parts found in a combustor typically

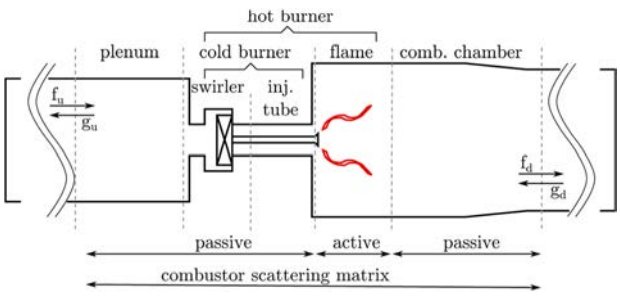

Fig. 1 Example of fragmenting a combustor into its acoustic elements

[1]Corresponding author.

have to be determined experimentally or numerically. Indeed, several studies deduced matrix coefficients for acoustically passive combustor parts of varying complexity, e.g., a single orifice [3], a tandem orifice [4], multiperforated liner plates [5], or a premixed nozzle [6]. The acoustic transfer behavior of swirl generators, which are an unavoidable part in swirl stabilized combustion systems, was numerically determined by Gikadi et al. [7] and Ni et al. [8]. A system of algebraic equations may be constructed from the collection of transfer (or scattering) matrices of the combustor elements. After closing this system with upstream and downstream boundary conditions, an "acoustic network model" or reduced order model (ROM) of the combustion system is obtained, which may be used, e.g., for linear stability analysis [9–11]. Experience has shown that this kind of analysis provides not only quantitative data on stability limits and dynamics of a combustion system but also important physical insight [9,11–16]. Several previous studies have concentrated on the transfer or scattering matrices of individual combustor elements such as a flame, a burner, a swirl nozzle, or a dissipative element [3–6,8,9,11,13,14,17–19]. The present study concerns in an integrated fashion a *combustor scattering matrix* that includes swirler, injection tube, and flame as well as parts of the combustion chamber, see Fig. 1.

In the absence of a flame, the passive parts of the combustor such as, e.g., swirler, area changes, or duct sections result in a certain acoustic transmission and reflection behavior of the combustor, described by the nonreactive or *cold* combustor scattering matrix. Under reacting conditions, the flame is an *active* element that introduces an additional degree of complexity. This applies in particular to swirl flames. Because of the swirling flow, the complex geometries involved, and the intricacies of flame dynamics with interaction of various physical processes [20], the assessed acoustic transfer relations will in general not be straightforward. The transfer matrix of a lean premixed gas turbine burner in a reactive or *hot* configuration was studied experimentally by Paschereit et al. [17,18]. Transfer matrix coefficients were measured by successive monofrequent excitation of the combustor flow with a two-source scheme. However, such *direct* measurement of a hot transfer matrix is very challenging and can be tedious. A careful calibration of the diagnostics is required for precise measurements of the acoustic variables and the downstream conditions in the reacting case are not conducive for precise measurements [14].

Therefore, alternative methods for determining the transfer matrix of a burner or combustor under hot conditions are desirable. One possibility is the use of large eddy simulation (LES) to *directly* deduce the combustor transfer or scattering matrix [13,19,21] from simulations with acoustic forcing, where a prescribed acoustic signal is imposed at the inlet or outlet of the LES domain. Considering that successive monofrequent excitation in LES entails very significant computational costs, the LES/system identification (SI) is the method of choice here. This approach is computationally efficient, as it allows to identify transfer functions or matrices over a range of frequencies from a single simulation with broadband acoustic forcing [22].

An indirect approach for determining a hot burner transfer matrix from a flame transfer function (FTF), which relates upstream velocity fluctuations to resulting heat release rate fluctuations, is proposed by Keller [9] and Polifke et al. [11]. Specifically, the hot burner transfer matrix is computed as the product of the transfer matrix of the cold burner and the transfer matrix of the flame, which is deduced from the Rankine–Hugoniot (RH) equations that describe the conservation of mass, momentum, and energy across an acoustically compact zone of heat release [9]. This *composition* method for the reactive configuration has been applied successfully in several studies [13–15] and is also employed in the present study: the FTF is coupled via the RH relations into a ROM of the full cold combustor, which is built from simpler acoustic elements (ducts, area jumps, flame element, …, see Fig. 1), in order to determine the hot combustor transfer matrix.

The *direct* as well as the *composed* approach come with certain advantages, but also limitations. The composed combustor scattering matrix is valid only for systems that respect the modeling assumptions of the RH+FTF coupling, such as, e.g., acoustic compactness of the flame and a dominant sensitivity of the flame to upstream velocity perturbations. The latter is not always the case for technically premixed flames. Moreover, simplifications due to the one-dimensional (1D) acoustics assumption are made in the composed approach. All these limitations are nonexistent in the direct approach, as all relevant effects are fully described within the LES. This means that, e.g., for noncompact or technically premixed flames, only the direct approach is applicable. On the other hand, if the composed approach is applicable, it requires significantly less computational effort than the direct approach. Even though both approaches require a computationally demanding LES in the first place, the identification of *four* frequency-dependent scattering matrix coefficients requires longer LES time series data for accurate estimation than *one* FTF model. More important though, as long as changes in the combustor geometry do not have an impact on the FTF, they may be easily taken into account in the respective element of the network model. So, once the FTF is identified, scattering matrices for a wide parameter space may be derived by a simple re-evaluation of the adapted ROM. In the direct approach, new LES runs need to be carried out if the geometry within the computational domain is changed.

The current work aims for a one-to-one comparison between the two different numerical methods of determining the scattering matrix of a turbulent swirl combustor in reacting conditions. This comparison provides valuable insight to which extent results of the two methods coincide for a case where the composed approach is applicable. Modeling results are also validated against and compared to experimental measurements of the FTF and the combustor scattering matrix. Note that a direct computation of a turbulent combustor scattering matrix with LES/SI constitutes a novelty and that a one-to-one comparison between the aforementioned methods is still lacking in literature for turbulent combustors.

Transfer and Scattering Matrices

Formally, the transfer matrix representation and the scattering matrix counterpart are mutually interchangeable. The transfer matrix defines the dynamic relation of the acoustic fields upstream and downstream of an element and is expressed in terms of primitive acoustic variables, i.e., the fluctuation of pressure p' and velocity u'

$$\begin{bmatrix} \frac{p'_d}{\overline{\rho c}} \\ u'_d \end{bmatrix} = \begin{bmatrix} T_{11} & T_{12} \\ T_{21} & T_{22} \end{bmatrix} \begin{bmatrix} \frac{p'_u}{\overline{\rho c}} \\ u'_u \end{bmatrix} \tag{1}$$

On the other hand, the scattering matrix is defined in terms of the characteristic waves or Riemann invariants

$$f = \frac{1}{2}\left(\frac{p'}{\overline{\rho c}} + u'\right) \tag{2a}$$

$$g = \frac{1}{2}\left(\frac{p'}{\overline{\rho c}} - u'\right) \tag{2b}$$

and relates the outgoing characteristic waves (f_d, g_u) to the incoming counterparts (f_u, g_d)

$$\underbrace{\begin{bmatrix} f_d \\ g_u \end{bmatrix}}_{\text{response}} = \begin{bmatrix} S_{11} & S_{12} \\ S_{21} & S_{22} \end{bmatrix} \underbrace{\begin{bmatrix} f_u \\ g_d \end{bmatrix}}_{\text{signal}} \tag{3}$$

As both representations are interchangeable, the scattering matrix coefficients can be computed from the transfer matrix coefficients by a simple algebraic transformation

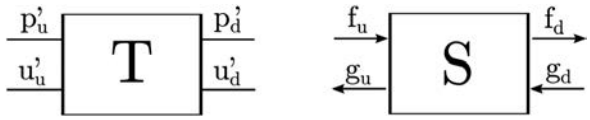

Fig. 2 Representation in terms of transfer matrix (left) and scattering matrix (right)

$$S_{11} = 2(T_{11}T_{22} - T_{12}T_{21})/D \tag{4a}$$

$$S_{12} = (T_{11} - T_{12} + T_{21} - T_{22})/D \tag{4b}$$

$$S_{21} = (-T_{11} - T_{12} + T_{21} + T_{22})/D \tag{4c}$$

$$S_{22} = 2/D \tag{4d}$$

with $D = T_{11} - T_{12} - T_{21} + T_{22}$.

As shown in Eq. (3) and Fig. 2, the scattering matrix coefficients S_{11} and S_{22} describe the transmission from upstream to downstream and *vice versa*. The scattering matrix coefficients S_{12} and S_{21} define the reflection of characteristic waves impinging from downstream and upstream, respectively. Compared to the transfer matrix representation, the scattering matrix representation respects the causality of the system. The characteristic waves f and g have a distinct propagation direction, which in turn allows to establish a causal relation between the input *signal* and the system's *response*, see Eq. (3). A certain input signal causes a certain response of the system. This in turn means that the present output of the system only depends on the present and previous inputs. Even though the transfer matrix is related to the scattering matrix by simple algebraic relations, see Eqs. (4*a*)–(4*d*), it does not respect causality since the primitive acoustic variables, in which the transfer matrix is expressed, do not have a distinct propagation direction. Thus, a strict separation between input *signal* and system's *response* is no longer possible. For further details on the causality of the respective representations, the reader is referred to Ref. [22].

Although only the scattering matrix respects causality, both representation exhibit certain advantages and disadvantages—so it makes sense to use both. On the one hand, the transfer matrix representation allows a fluid dynamical interpretation of its coefficients in terms of inertia and losses. The T_{22} coefficient, which relates upstream to downstream velocity perturbations, mainly characterizes the thermoacoustic interaction [14]. On the other hand, the scattering matrix allows to set up an acoustic energy balance determining the amplification or damping across the scattering object [15,19]. Based on that, the system's stability may be judged or possible feedback mechanism may be revealed [19]. The scattering matrix representation is also helpful when it comes to the definition of a combustion noise source vector, as shown by Paschereit et al. [18].

In regard to the costs of determination, both representations are comparable. In experiments, often the transfer matrix is measured [12,14,17,18,23] since the primitive acoustic variables p' and u' can be assessed directly. In the LES/SI approach, the scattering matrix is easier to identify as it respects causality and allows thus to apply a causal finite impulse response (FIR) model [19]. In the current work, the comparison between experimental and numerical results is presented in terms of the scattering matrix representation, since it provides a straight forward interpretation of the acoustic processes involved compared to the one given by the transfer matrix. Hence, the experimentally measured transfer matrices are transformed into the scattering matrix representation via Eqs. (4*a*)–(4*d*).

Experimental Setup

The investigated swirl combustor, shown in Fig. 3, is located at EM2C laboratory, Paris. A mixture of methane and air is injected

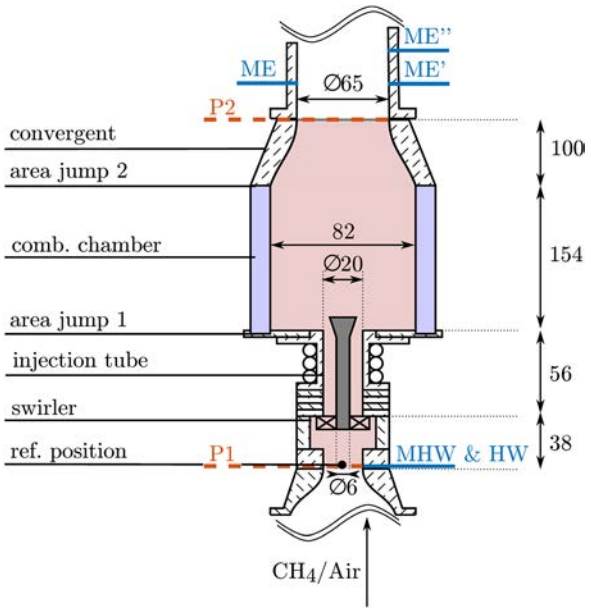

Fig. 3 Sketch of the EM2C turbulent swirl combustor. Dimensions are given in millimeter.

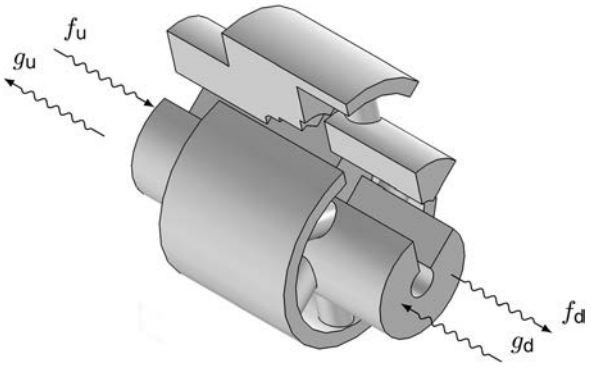

Fig. 4 Radial swirler geometry

in a tranquilization box (not shown in Fig. 3). A loudspeaker (Monacor SP-6/108PRO - 100 W RMS) is added at the bottom of the tranquilization box and generates the acoustic forcing corresponding to 10% of the mean inlet velocity. A plenum followed by a converging nozzle (contraction ratio: 8.73) generates a laminar flow with a top-hat velocity profile in the reference plane where a hot-wire probe HW (Dantec Dynamics Mini-CTA 54T30 with a 55P16 probe) is used to measure the velocity signal u'_u (in the top-hat region of the profile). At the same location, a microphone MHW (Bruel & Kjaer 4938) is used to measure the acoustic pressure fluctuations p'_u. A swirler (see Fig. 4) comprising six off-centered radial vanes of radius $R = 3$ mm (contraction ratio: 7.41) produces a flow with a swirl number $S = 0.8$ that was measured by Laser Doppler Velocimetry in the confinement chamber, just after the injector tube exit. A bluff body of conical shape is used to stabilize the flame inside the confinement chamber. A second convergent (contraction ratio: 2.03) is placed at the top of the combustion chamber, followed by an exhaust tube. The flame investigated in this study is a perfectly premixed methane/air flame with an equivalence ratio $\phi = 0.82$ and a thermal power of 5.5 kW. The associated bulk velocity at the hot-wire location is $u_b = 5.4$ m/s in a tube of diameter $D = 22$ mm, yielding a Reynolds number of approximately Re ≈ 7000.

Three microphones (Bruel & Kjaer 4938) are mounted on water-cooled waveguides in the hot gases region. The small

distortions induced by these waveguides while propagating the acoustic waves are corrected through the use of their transfer function that was determined previously. The first two microphones, ME and ME′ in Fig. 3, are located directly opposed in the exhaust tube, 35 mm downstream of the second convergent. A third microphone, ME″ in Fig. 3, is located 85 mm downstream the second convergent. In addition to the acoustic pressure fluctuations p'_d measured by ME″ in the downstream region, the three-microphone method [24] is used to reconstruct the acoustic velocity fluctuations u'_d at the same axial position. In order to improve the signal-to-noise ratio, all experiments are made twice: one in the original configuration presented in Fig. 3 and another one with the microphones ME′ and ME″ switched. Moreover, coherence functions are also adopted when reconstructing u'_d [24].

Equation system (1) contains four unknowns T_{11}, T_{12}, T_{21}, T_{22} but only two equations, which explains why two independent acoustic states are needed. In most experiments, the two source method is used [14,17,18,23]. Here, the two loads method is retained [25]. Both methods are based on the same physical process, namely a modification of one or more acoustic boundary conditions. For reactive conditions, the two loads used in this study consist of an exhaust tube of length $L = 220$ mm and the same exhaust tube with a perforated plate added at the top of it. For nonreactive conditions, the first load consists again of an exhaust tube of length $L = 220$ mm, whereas the second load makes use of two exhaust tubes with a total length of $L = 440$ mm. The configurations used in both cases are independent for all frequencies of interest.

Large Eddy Simulation/System Identification Approaches

Two different approaches are applied to obtain the scattering matrix for cold and hot conditions. First, in the direct approach, the scattering matrix is directly computed from the LES time series. Second, only the FTF is identified from LES generated time series data. The identified FTF is then coupled via the RH jump equations into a ROM of the passive combustor. The hot combustor scattering matrix is consequently obtained from the composed model. Before the individual approaches are described in detail, the LES setup and the SI method as used in both approaches are introduced.

Large Eddy Simulation/System Identification Methodology. Compared to the studies of Polifke and coworkers [19,21], which were based on unsteady Reynolds-averaged Navier–Stokes (RANS) simulation, a compressible LES is used in the present study. Giauque et al. [26] showed that LES provides a better estimation of the time lag between heat release fluctuations and upstream velocity fluctuations than a RANS computation. Similarly, Tay-Wo-Chong et al. [27] stated that LES yields more accurate estimates of the FTF than unsteady RANS.

The LES is performed with the solver AVBP [28]. The fully compressible Navier–Stokes equations are solved on an unstructured grid consisting of approximately 19 million cells with a maximum cell size of 0.6 mm in the flame region. The shaded area in Fig. 3 indicates the domain resolved by the LES. The rather complex geometry of the swirler shown in Fig. 4 is fully resolved by the LES. No geometrical simplifications are applied. The six off-centered radial swirler vanes, which have a diameter of 6 mm, are resolved by approximately 18 cells in the diameter that are refined toward the walls. In total, the section containing the swirler is resolved by about 4 million cells.

For handling subgrid scales in the LES, the WALE model is applied [29] due to its capacity to recover turbulent subscale statistics in near wall regions. Turbulence–flame interaction is taken into account by the dynamically thickened flame [30] model with seven cells resolving the laminar flame thickness. The chemistry of the perfectly premixed methane/air flame is described by a

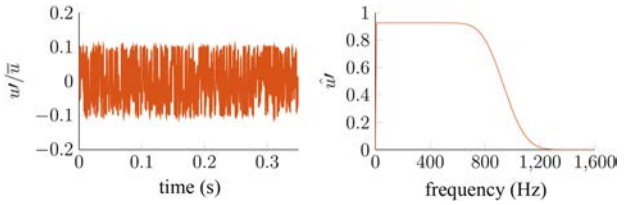

Fig. 5 Forcing signal: time series (left) and spectral distributions (right)

global two-step scheme. Nonreflecting boundary conditions are applied at the inlet and outlet by using plane wave masking [31]. For further details and a proper validation of the LES setup, the reader is referred to Ref. [32].

Instead of computing discrete values of the scattering matrix or the FTF by forcing the flow monofrequently and repeatedly over a certain frequency range, the flow is forced with an acoustic broadband signal. As forcing signal, a wavelet type signal is used, see Fig. 5. The forcing amplitude is set to 10% of the mean inlet velocity and the signal has a constant power spectral density and a low auto-correlation up to the cut-off frequency of approximately 800 Hz. Having no peak values in the broadband forcing signal above 10% of the mean inlet velocity ensures that the flame response remains in the linear regime. Two independent data sets with a respective time series length of 350 ms are created. The chosen time series length of 350 ms represents a compromise. Generally, longer time series yield a more accurate identification but are also computationally more expensive. A value of 350 ms results thus from best practice as it allows a proper and robust identification with reasonable computational effort. For the first data set, the acoustic forcing signal is applied at the inlet (f_u) and the resulting signals are extracted from the measurement planes P1 (g_u) and P2 (f_d). The second data set is generated analogously by applying a downstream forcing (g_d) and measuring the time series (g_u, f_d).

From the generated time series data, models can be identified that relate respective inputs and outputs. Depending on the choice of input and output signals, the four scattering matrix coefficients or the FTF can be identified. In both cases, every transfer expression is modeled by a causal FIR, which relates present outputs to prior inputs [27,33,34]. Note that for a noncausal system representation, as, e.g., the transfer matrix, a noncausal FIR model needs to be applied that requires both prior and future inputs in order to estimate the model output [13]. The causal FIR model reads as

$$y(t) = \sum_{i=0}^{n_b} b_i\, x(t - i\Delta t) + e(t) \tag{5}$$

Herein, the model output $y(t)$ is computed by convoluting the prior inputs $x(t - i\Delta t)$ and the FIR coefficients b_i. The number of prior input samples that are taken into account via the impulse coefficients b_i and thus the length of the FIR are specified by the model order n_b. Conversely, this means that the model order n_b determines how many model FIR coefficients b_i have to be estimated from the time series data. The higher the chosen model order n_b, the longer the time series needed for an accurate and robust identification of the respective FIR coefficients b_i. The term $e(t)$ represents a white noise perturbation on the output $y(t)$.

Direct Approach for Scattering Matrix. In the direct approach, the characteristic waves f and g are extracted from the LES measurement planes P1 and P2, see Fig. 3. These two measurement planes coincide with the inlet and the outlet of the LES domain and contain all combustor parts shown in Fig. 3 in between them. Note that the location of the downstream measurement ME″ does not coincide with the measurement plane P2 in the LES domain. This discrepancy stems from the fact that the

same LES setup is used as in Ref. [32], for which the LES was validated. However, the need in the current study of properly measuring the acoustic fluctuations downstream requires the test rig to be equipped with an additional pipe that contains the mounted microphones ME, ME′, and ME″ (see Fig. 3). Since the additional pipe has a constant cross section area, its only effect on the measured acoustic waves is the introduction of an additional time lag compared to the plane P2. To take this into account and to guarantee a proper comparison between measurements and numerical results, the numerically extracted time series in the direct approach are shifted by the aforementioned time lag in a first postprocessing step. This has an influence on the phase of the computed scattering matrix coefficients from the direct approach. The time lag Δt can be computed via the distance between the numerical measurement plane P2 and the microphone ME″ $\Delta x = 0.085$ m and the respective speed of sound c_c (nonreactive case) or c_h (reactive case). In order to separate acoustic from turbulent fluctuations, a characteristics-based filter [35] is applied, which improves the quality of the SI. Flame dynamics, flame-acoustic interactions, as well as acoustic propagation in the complex combustor geometry are directly resolved by the LES. From the upstream forced data set, the scattering matrix coefficients S_{11} and S_{21}, which describe the reflection and transmission of characteristic waves impinging from upstream, are directly identified via the SI procedure. Analogously, the coefficients S_{12} and S_{22} are estimated from the data set with downstream forcing applied.

In theory, it is also possible to get the four scattering matrix coefficients from one single data set, in which independent upstream and downstream forcing is applied simultaneously. Although this technique yielded accurate results for cold conditions, unsatisfactory results were obtained in the reactive case for a time series length of 350 ms. One possible reason might be that the generated time series was too short in the reactive case for the simultaneously identification of all four scattering matrix coefficients. Moreover, other than in the nonreactive case, combustion noise corrupts the time series data. This means that acoustic fluctuations, generated by turbulent velocity perturbations impinging on the flame front, overlay the forced flame response resulting from the acoustic broadband forcing. It is emphasized that this issue applies not only for a broadband forcing method but also in cases of a monofrequent forcing of the flow. The totally recorded acoustic fluctuations may thus be distinguished into two contributions: First, a contribution that results from the acoustic forcing and second, a contribution that stems from turbulent combustion noise. Note, the second contribution is by definition *uncorrelated* to the deterministic flame response and hinders thus the identification in hot conditions [16]. For consistency, two independent data sets (upstream and downstream forcing) are thus used in the current study for both reactive and nonreactive conditions.

Flame Transfer Function + Reduced Order Model Approach. The ROM is based on a linear acoustic network model as it was used, e.g., in Refs. [36] and [37]. It describes the main elements of the combustor and is implemented in the open-source acoustic network tool taX [38]. The model is depicted in Fig. 6. The geometrical and thermodynamical parameters of the ROM are summarized in Table 1.

Every element of the linear network model is defined by a 2×2 transfer matrix that relates the upstream characteristic waves f_u and g_u to the characteristic waves f_d and g_d downstream of the element. Note that instead of using a network model based on transfer matrices, the respective elements could also be described equivalently by their scattering matrix. The connection of two elements would then be either realized by using the Redheffer Star-Product [39], which combines two scattering matrices to form an overall scattering matrix through simple algebraic combination of the respective subelements, or by converting the scattering matrices into a transfer matrix representation before connecting them by simple concatenation.

Duct sections like the injection tube or the convergent part downstream of the combustion chamber only introduce a time lag between the upstream and the downstream characteristic waves and are described as

$$\begin{bmatrix} f_d \\ g_d \end{bmatrix} = \begin{bmatrix} e^{-\mathrm{i}\omega l/\bar{c}} & 0 \\ 0 & e^{\mathrm{i}\omega l/\bar{c}} \end{bmatrix} \begin{bmatrix} f_u \\ g_u \end{bmatrix} \tag{6}$$

with ω as angular frequency, l as respective duct length, and $\bar{c}$ as the mean speed of sound in the respective duct section. The area jumps within the network model are described in a simplistic manner

$$\begin{bmatrix} f_d \\ g_d \end{bmatrix} = \begin{bmatrix} 1 + A_u/A_d & 1 - A_u/A_d \\ 1 - A_u/A_d & 1 + A_u/A_d \end{bmatrix} \begin{bmatrix} f_u \\ g_u \end{bmatrix} \tag{7}$$

wherein A_u/A_d describes the area ratio from upstream to downstream section. The area jumps are assumed to be loss free and have no end correction.

Since the complex radial swirler geometry is only insufficiently approximated by simple duct and area jump elements, it is replaced by a 2×2 scattering matrix that is converted into a transfer matrix representation. The swirler scattering matrix is

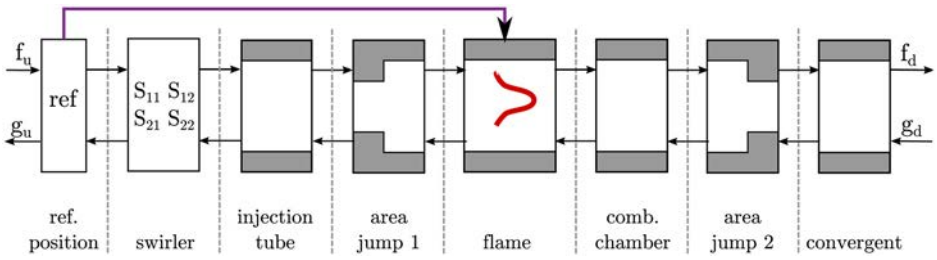

Fig. 6 Reduced order model: the swirler is replaced by an identified scattering matrix

Table 1 Summary of the geometrical and thermodynamical parameters used in the ROM

Injection tube	Flame	Comb. chamber	Convergent
$l_{\mathrm{inj}} = 0.034$ m $A_{\mathrm{inj}} = 3.52 \times 10^{-4}$ m^2 $u_{\mathrm{inj}} = 7.1$ m/s	$T_c = 293$ K $T_h = 1550$ K $\rho_c = 1.205$ kg/m^3 $\rho_h = 0.235$ kg/m^3	$l_{cc} = 0.154$ m $A_{cc} = 6.73 \times 10^{-3}$ m^2	$l_{\mathrm{conv}} = 0.185$ m $A_{\mathrm{conv}} = 3.32 \times 10^{-4}$ m^2

identified similarly to the direct approach: the flow in a LES, whose domain comprises only the swirler geometry, is simultaneously forced from upstream and downstream by a broadband acoustic signal. From the generated time series, the scattering matrix is determined via SI techniques. For brevity, the resulting swirler scattering matrix is not explicitly shown here.

The FTF is identified from a time series of velocity fluctuations at the reference position u'_{ref}, which coincides with the experimental reference position as shown in Fig. 3, and total heat release rate fluctuations $\dot{Q}'$, both extracted from the upstream forced data set

$$F(\omega) = \frac{\dot{Q}'/\overline{\dot{Q}}}{u'_{\mathrm{ref}}/\overline{u}} \tag{8}$$

The comparison between the experimentally measured FTF and the one deduced from the LES/SI approach is depicted in Fig. 7. The error bars for the measured FTF are deduced from three experimental data sets for the same operating conditions and represent the maximum error in reproducibility of the experiment. The model order of the identified FTF is equal to $n_b = 30$.

In the following step, the identified FTF is coupled into the ROM via the linearized RH equations that describe the jump conditions across a thin zone of heat release at low Mach number

$$p'_d = p'_u \tag{9a}$$

$$u'_d = u'_u + \frac{(\gamma-1)}{\gamma \bar{p} A}\,\dot{Q}' \tag{9b}$$

where γ represents the heat capacity ratio and A the cross section area of the flame region. By inserting Eqs. (2*a*) and (2*b*) into the RH jump equations (9*a*) and (9*b*), the transfer matrix across the thin reaction zone is obtained as

$$\begin{bmatrix} f_d \\ g_d \end{bmatrix} = \frac{1}{2}\begin{bmatrix} \xi+1 & \xi-1 \\ \xi-1 & \xi+1 \end{bmatrix}\begin{bmatrix} f_u \\ g_u \end{bmatrix} + \frac{1}{2}\frac{A_u}{A_d}\theta F(\omega)\begin{bmatrix} 1 & -1 \\ -1 & 1 \end{bmatrix}\begin{bmatrix} f_{\mathrm{ref}} \\ g_{\mathrm{ref}} \end{bmatrix} \tag{10}$$

with ξ denoting the specific acoustic impedance between burnt and unburnt gases $\xi = (\rho_c c_c)/(\rho_h c_h)$ and θ specifying the temperature ratio $\theta = T_h/T_c - 1$.

The coupling of the FTF into the ROM is indicated by the additional arrow in Fig. 6. Note that this coupling approach only holds if certain constraints are respected: (1) The flame is assumed to be compact with respect to the acoustic wavelength considered. (2) Influence of pressure fluctuations on the flame response is insignificant. For the given working conditions, the flame length is about $l_f \approx 0.04$ m. The scattering matrices are evaluated in the low frequency region up to a frequency of 400 Hz resulting in a maximum Helmholtz number of $\mathrm{He} < 0.05$. The Helmholtz number is thus much smaller than unity, implying that the flame may be assumed to be acoustically compact. As mentioned in the experimental description, methane and air are already premixed before their injection into the plenum. For perfectly premixed flames, velocity sensitivity is a valid assumption [40]. From these considerations, it is concluded that the FTF+ROM approach should provide valid predictions for the scattering matrix coefficients in the hot configuration.

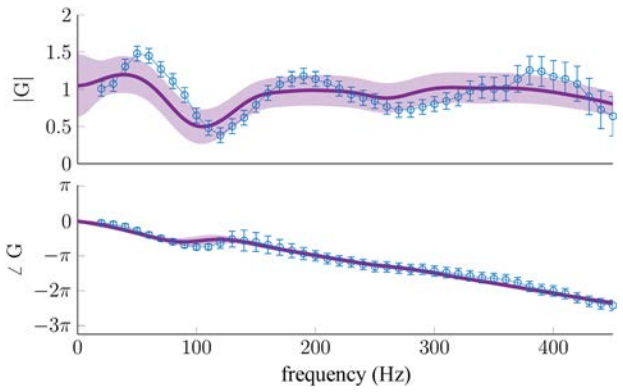

Fig. 7 Comparison between measured FTF (○) with respective error bars and FTF from LES/SI (——). The shaded area represents the 95% confidence interval of the identified FTF.

Results

First, the combustor scattering matrix from experiment, the direct approach, and the ROM prediction are compared for the cold case. This validates the LES/SI procedure and the ROM of the cold combustor to a certain extent and derives the results of the reactive case on a solid basis. In a second step, the hot configuration is investigated.

Nonreactive Case. Figure 8 depicts the four scattering matrix coefficients deduced from experiment (○), the direct LES approach without combustion (——), and the ROM prediction for the cold configuration (——). In the ROM, the downstream temperature T_h is set equal to the upstream temperature T_c resulting in $\theta = 0$. The second term on the r.h.s in Eq. (10) thus vanishes: the flame does not have any influence. In the direct approach, the model order for each of the four scattering matrix coefficients is set to $n_b = 10$. The confidence intervals for the direct approach that come from the SI procedure are not shown in Fig. 8. Due to the low model order of $n_b = 10$ and the high signal-to-noise ratio, the 95%

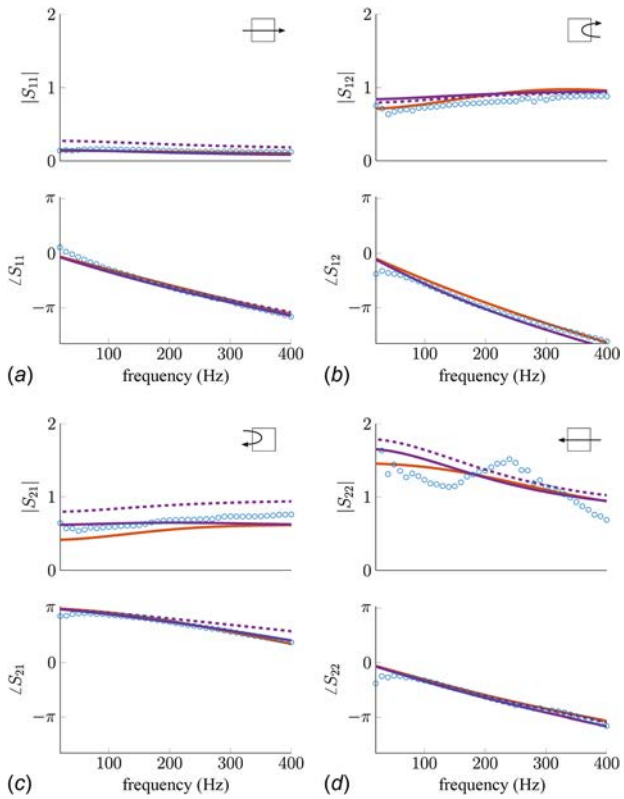

Fig. 8 Combustor scattering matrix for cold conditions. Experiment (○), direct LES approach (——), passive ROM (——) and passive ROM without swirler (- - -). (*a*) S_{11}, (*b*) S_{12}, (*c*) S_{21}, and (*d*) S_{22}.

confidence intervals of the estimated scattering coefficients are very small and could hardly be recognized in Fig. 8.

Considering the two reflection coefficients S_{12} and S_{21} as well as S_{11}, i.e., the transmission coefficients from upstream to downstream all three methods are in fairly good agreement. In particular, the phase matches excellently. On the other hand, the absolute values exhibit subtle differences. In contrast to the ROM, the direct LES approach takes acoustic losses into account. Therefore, the coefficients' magnitudes obtained by the direct LES approach are slightly smaller than the ones from the ROM. It can be observed that the magnitude of the transmission coefficient from downstream to upstream S_{22} exceeds unity for low frequencies. This results from the cross section area ratio between downstream measurement plane P2 and the upstream measurement plane P1 that is also above unity, see Fig. 3. Due to mass conservation, the ratio g_u/g_d, which is exactly described by the S_{22} coefficient, becomes larger than unity. For the same reason, the transmission coefficient S_{11} is distinctively below unity. The magnitude of the reflection coefficients S_{12} and S_{21} is of order unity. This strong reflection within the combustor geometry is caused by the large area jump between the injection tube and the combustion chamber, denoted as "area jump 1" in Fig. 6. An evaluation of its scattering behavior, see Eq. (7), shows that the largest parts of the incoming waves are reflected, whereas only a small part is transmitted across the area jump. Even though the phase of all three methods matches well for the transmission coefficient S_{22}, the variations measured in the absolute value are observed neither by the direct LES approach nor by the ROM. This discrepancy might be caused by inaccuracies in describing the acoustic transmission from the combustion chamber into the injection tube. However, the general trend and the magnitude of $|S_{22}|$ are in fairly good agreement for all three methods.

To show the effect of the swirler scattering matrix within the ROM, it was replaced by a simple duct element having the same length as the swirler element, see (- - -) in Fig. 8. Compared to the ROM containing the swirler scattering matrix (——), a larger deviation to experimental results and to the direct approach is observable. It can be concluded that the use of a nontrivial swirler scattering matrix increases the accuracy of the ROM.

Overall, several conclusion may be drawn from the results of the cold configuration: (1) The compressible LES correctly describes the acoustic propagation within the complex combustor geometry, allowing the LES/SI procedure to extract all four scattering matrix coefficients from the broadband time series data over a range of frequencies. (2) The ROM based on a linear network model is able to correctly reproduce the main features of the cold scattering matrix. This means that the passive combustor parts are modeled by the ROM with sufficient accuracy, despite the simplifications made such as 1D acoustics or the simplified geometry. (3) The area jump between injection tube and combustion chamber reflects most of the incoming waves. (4) The swirler is acoustically not completely transparent. (5) The direct LES approach and the ROM correctly capture the time lag between ingoing and outgoing characteristic waves as the phase is in excellent agreement with experimental measurements. This in turn means that the time lag correction due to the differing measurement locations in experiment and direct approach is valid and yields satisfying results.

Conclusions (1) to (5) put the following study of the hot configuration on a solid basis and allow to exclude some reasons for any discrepancies between the methods in the reactive configuration.

Reactive Case. Figure 9 shows the scattering matrix coefficients for the reactive configuration obtained by experiment (○), the direct LES approach with combustion (——), the FTF+ROM approach (——), and a ROM with *passive flame* (- - -). In the last case, the temperature increase across the flame is taken into account, but the unsteady heat release as represented by the FTF is not, i.e., the flame is inactive. For the direct approach, the FIR model order is now increased to $n_b = 30$ for each of the four

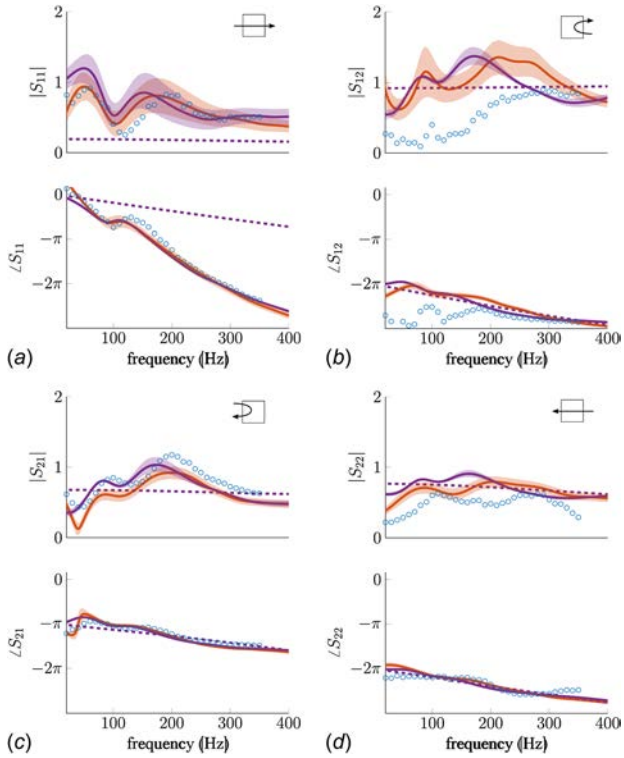

Fig. 9 Combustor scattering matrix for hot conditions. Experiment (○), direct LES approach (——) and FTF+ROM (——) and ROM with passive flame (- - -). The shaded areas describe the 95% confidence interval of the respective numerical approach. (*a*) S_{11}, (*b*) S_{12}, (*c*) S_{21}, and (*d*) S_{22}.

scattering matrix coefficients, as the presence of the flame results in a more complex scattering behavior and the flame time lag is quite large compared to acoustic scales.

The direct and the FTF+ROM approaches yield results for the four scattering matrix coefficients that are largely consistent with each other and show overall satisfactory agreement with measurements. However, the downstream reflection coefficient S_{12} (top-right subplot) exhibits pronounced discrepancies between the numerical results and experiment, especially in the low-frequency region. A possible explanation for the discrepancy might be that the acoustic signals in experiment as well as in LES are overlaid by combustion noise emitted from the turbulent flame, which is known to be active predominantly in the low-frequency region. One should expect that combustion noise is most detrimental for determination of the S_{12} coefficient, since it describes reflection of a wave g_d coming from downstream into a wave f_d propagating in the downstream direction. For the determination of this coefficient, both signals are extracted downstream of the flame in the combustion chamber, where combustion noise amplitudes higher than in the plenum must be expected.[2] Consistently, the measurement variation observed is largest in the S_{12} coefficient.

Note that forcing amplitudes should not be increased arbitrarily, in order to avoid a nonlinear flame response. A decrease in the signal-to-noise is thus unavoidable, which worsens the reliability of the SI results. Indeed, the confidence intervals of the scattering coefficient S_{12} estimated with the direct approach are quite wide, see Fig. 9(*b*). However, the confidence intervals are not wide enough to account for the discrepancies between simulation and experiment. One should also consider that in the experiments, the acquisition time per frequency measurement was fixed. Thus, measurements for higher frequencies are statistically more

[2]In the cold configuration, the only physical noise source is aero-acoustic noise, which is rather small for low Mach numbers. The signal-to-noise ratio is thus favorable in this case, yielding reliable results also for S_{12}.

reliable, as more forcing cycles are recorded and the stochastic noise contribution becomes less significant. Indeed, the agreement between numerical predictions and measurements improves with frequency. Conversely, with decreasing forcing frequency, fewer and fewer cycles were recorded and agreement deteriorates. Differences in measurement principle—two-source with broad-band forcing and nonreflection boundary conditions in LES/SI versus two-load with monofrequent forcing and partial reflection in experiment—may also contribute to the discrepancies.

The 95% confidence intervals shown for the FTF+ROM approach are determined by propagating the uncertainties in FTF magnitude (see Fig. 7) through the ROM. By comparing the width of confidence intervals obtained with the FTF+ROM approach, it becomes evident that in particular the upstream transmission coefficient S_{11} exhibits significant uncertainties. The interpretation of this behavior is the following: If the flow is forced upstream, significant velocity perturbations are generated at the reference position, see Fig. 6. Via the FTF and the RH coupling, these fluctuations cause acoustic waves at the flame position, see Eq. (10). On the other hand, due to the aforementioned reflective area jump in between the injection tube and the combustion chamber (area jump 1 in Fig. 6), only a small part of the initial forcing signal reaches the outlet of the combustor. It follows that the signal at the outlet should be dominated by the acoustic waves generated at the flame position caused by velocity perturbations at the reference position. These arguments are corroborated by the following observations: (1) S_{11} as predicted by the ROM with passive flame (- - -) differs strongly from the prediction with active flame, (2) the magnitude of S_{11} shows a similar succession of local maxima and minima as the FTF at corresponding frequencies, (3) the phase of S_{11} is dominated by the flame time lag and not by the acoustic scales (as it is the case for the ROM with passive flame). Consequently, uncertainties in FTF identification impact noticeably the prediction of the S_{11} transmission coefficient.

The impact of the flame dynamics on the remaining scattering coefficients is weaker. The coefficients are closer in magnitude to the predictions of the ROM with passive flame (- - -) while the phase is dominated by acoustic time scales and matches thus the phase of the ROM with passive flame. This can be explained again through the reflective area jump between the injection tube and the combustion chamber. If the flow is forced from downstream, only a small portion of the acoustic forcing signal reaches the reference position upstream, since the largest part of the signal is reflected at the area jump. Accordingly, the contribution of the flame generated acoustic waves remains relatively small. The impact of the flame on the scattering coefficients S_{12} and S_{22} is only moderate. The same holds for the upstream reflection coefficient S_{21}. Even though the flame response is considerable—the upstream acoustic forcing directly causes velocity perturbations at the reference position—only a small part of the upstream traveling acoustic waves generated at the flame position reach again the upstream end of the combustor.

To conclude, uncertainties in the determination of the scattering coefficients in the FTF+ROM approach are largest, where the flame modulates the passive scattering matrix the most.

Summary and Conclusions

The aim of this paper is a one-to-one comparison between two alternative numerical approaches for deducing the scattering matrix of a turbulent swirl combustor under nonreactive as well as reactive conditions. The respective approaches combine LES, SI and ROM. Numerical results for the *cold* and *hot* combustor scattering matrix are compared against each other and against experiment. The first approach identifies scattering matrix coefficients directly from broadband time series data that are generated by a compressible LES with broadband forcing. The second approach identifies only the FTF from the compressible LES, which is then coupled into a ROM of the combustor acoustics via the RH equations in order to compose the scattering matrix.

The results for the nonreactive scattering matrix show excellent agreement between simulation and experiment. This suggests that the 1D acoustic assumption made in the ROM is justified. Moreover, it becomes evident that the radial swirler is acoustically not completely transparent. Consequently, the use of nontrivial swirler scattering matrix further increases the accuracy of the ROM.

The scattering matrices for the reactive setup also exhibit satisfactory agreement, even though the downstream reflection coefficient S_{12} shows a distinct discrepancy between the numerical predictions—which coincide with each other—and the measurements. Possible reasons for the discrepancies are the small signal-to-noise ratio of the time series data extracted in the burnt gas region and the finite time series length available. In the direct approach, a finite time series length introduces uncertainties in the identification process in particular at low frequencies, in experiment fewer cycles can be recorded for low forcing frequencies due to the fixed acquisition time. Nonetheless, considering the good agreement between the two quite different numerical approaches and the overall good agreement with the measurements of the nonreactive and the reactive scattering matrix, it is principally shown that both numerical approaches are capable of determining the scattering matrix of a complex combustor. Moreover, the comparison to the ROM with a passive flame highlights the impact of the flame on the acoustic scattering matrix of the combustor. It is shown that the transmission coefficient from upstream to downstream S_{11} is dominated by the flame dynamics, i.e., the FTF.

The composed approach yields accurate results, as long as the constraints of the coupling between FTF and ROM via the Rankine–Hugoniot equations are respected. The perfectly premixed flame investigated in this study is indeed predominantly velocity sensitive and acoustically compact. One may conclude that the other simplifications implied by the composed approach, such as 1D acoustics or a constant temperature distribution in the hot gas region, do not introduce significant errors. The applicability of the composed approach in this case would allow the computationally efficient determination of the combustor scattering matrix for a wide parameter space, as changes could be easily implemented in the ROM. However, there are situations in which the constraints of the composed approach are no longer respected. The mixture might be technically premixed introducing a pressure sensitivity of the flame or the flame might be no longer acoustically compact. In these situations, the more general direct LES approach would be necessary to accurately predict the reactive scattering matrix, as it allows to drop the constraints of the composed approach. All relevant mechanisms are directly resolved within the compressible LES.

The comparisons and analysis carried out in this study thus provide valuable insight to which extent both numerical methods yield coinciding results for a configuration, where the composed approach is applicable.

Funding Data

- The authors acknowledge financial support by the German Research Foundation DFG, project PO 710/16-1 and by the Agence Nationale de la Recherche, NOISEDYN project (ANR-14-CE35-0025-01). This project also has received funding from the European Union's Horizon 2020 research and innovation programme under the Marie Sklodowska-Curie grant agreement No 643134. Moreover, the author gratefully acknowledges the Gauss Centre for Supercomputing e.V. for funding this project by providing computing time on the GCS Supercomputer SuperMUC at Leibniz Supercomputing Centre.

References

[1] Lefebvre, A. H., 1999, *Gas Turbine Combustion*, 2nd ed., Taylor & Francis, Philadelphia, PA.

[2] Munjal, M. L., 2014, *Acoustics of Ducts and Mufflers*, 2nd ed., Wiley, Chichester, UK.

[3] Su, J., Rupp, J., Garmory, A., and Carrotte, J., 2015, "Measurements and Computational Fluid Dynamics Predictions of the Acoustic Impedance of Orifices," J. Sound Vib., **352**, pp. 174–191.

[4] Sovardi, C., Aurégan, Y., and Polifke, W., 2016, "Parametric LES/SI Based Aeroacoustic Characterization of Tandem Orifices in Low Mach Number Flows," Acta Acust. Acust., **102**(5), pp. 793–803.

[5] Andreini, A., Bianchini, C., Facchini, B., Peschiulli, A., and Vitale, I., 2012, "LES for the Evaluation of Acoustic Damping of Effusion Plates," ASME Paper No. GT2012-68792.

[6] Yoon, C., Graham, O., Han, F., Kim, K., Maxted, K., Caley, T., and Lee, J. G., 2017, "LES-Based Scattering Matrix Method for Low-Order Acoustic Network Models," ASME Paper No. GT2017-65123.

[7] Gikadi, J., Ullrich, W. C., Sattelmayer, T., and Turrini, F., 2013, "Prediction of the Acoustic Losses of a Swirl Atomizer Nozzle Under Non-Reactive Conditions," ASME Paper No. GT2013-95449.

[8] Ni, F., Miguel-Brebion, M., Nicoud, F., and Poinsot, T., 2017, "Accounting for Acoustic Damping in a Helmholtz Solver," AIAA J., **55**(4), pp. 1205–1220.

[9] Keller, J. J., 1995, "Thermoacoustic Oscillations in Combustion Chambers of Gas Turbines," AIAA J., **33**(12), pp. 2280–2287.

[10] Dowling, A. P., 1995, "The Calculation of Thermoacoustic Oscillation," J. Sound Vib., **180**(4), pp. 557–581.

[11] Polifke, W., Paschereit, C. O., and Döbbeling, K., 2001, "Constructive and Destructive Interference of Acoustic and Entropy Waves in a Premixed Combustor With a Choked Exit," Int. J. Acoust. Vib., **6**(3), pp. 135–146.

[12] Schuermans, B., Bellucci, V., Guethe, F., Meili, F., Flohr, P., and Paschereit, O., 2004, "A Detailed Analysis of Thermoacoustic Interaction Mechanisms in a Turbulent Premixed Flame," ASME Paper No. GT2004-53831.

[13] Bothien, M., Lauper, D., Yang, Y., and Scarpato, A., 2017, "Reconstruction and Analysis of the Acoustic Transfer Matrix of a Reheat Flame From Large-Eddy Simulations," ASME Paper No. GT2017-64188.

[14] Alemela, P. R., Fanaca, D., Ettner, F., Hirsch, C., Sattelmayer, T., and Schuermans, B., 2008, "Flame Transfer Matrices of a Premixed Flame and a Global Check With Modelling and Experiments," ASME Paper No. GT2008-50111.

[15] Laera, D., Gentile, A., Camporeale, S. M., Bertolotto, E., Rofi, L., and Bonzani, F., 2015, "Numerical and Experimental Investigation of Thermo–Acoustic Combustion Instability in a Longitudinal Combustion Chamber: Influence of the Geometry of the Plenum," ASME Paper No. GT2015-42322.

[16] Silva, C. F., Merk, M., Komarek, T., and Polifke, W., 2017, "The Contribution of Intrinsic Thermoacoustic Feedback to Combustion Noise and Resonances of a Confined Turbulent Premixed Flame," Combust. Flame, **182**, pp. 269–278.

[17] Paschereit, C. O., and Polifke, W., 1998, "Investigation of the Thermo-Acoustic Characteristics of a Lean Premixed Gas Turbine Burner," ASME Paper No. 98-GT-582.

[18] Paschereit, C. O., Schuermans, B. B. H., Polifke, W., and Mattson, O., 2002, "Measurement of Transfer Matrices and Source Terms of Premixed Flames," ASME J. Eng. Gas Turbines Power, **124**(2), pp. 239–247.

[19] Gentemann, A., and Polifke, W., 2007, "Scattering and Generation of Acoustic Energy by a Premix Swirl Burner," ASME Paper No. GT2007-27238.

[20] Candel, S., Durox, D., Schuller, T., Bourgouin, J. F., and Moeck, J. P., 2014, "Dynamics of Swirling Flames," Annu. Rev. Fluid Mech., **46**(1), pp. 147–173.

[21] Polifke, W., Poncet, A., Paschereit, C. O., and Döbbeling, K., 2001, "Reconstruction of Acoustic Transfer Matrices by Instationary Computational Fluid Dynamics," J. Sound Vib., **245**(3), pp. 483–510.

[22] Polifke, W., 2014, "Black-Box System Identification for Reduced Order Model Construction," Ann. Nucl. Energy, **67C**, pp. 109–128.

[23] Fischer, A., Hirsch, C., and Sattelmayer, T., 2006, "Comparison of Multi-Microphone Transfer Matrix Measurements With Acoustic Network Models of Swirl Burners," J. Sound Vib., **298**(1–2), pp. 73–83.

[24] Chung, J. Y., and Blaser, D. A., 1980, "Transfer Function Method of Measuring In-Duct Acoustic Properties—II: Experiment," J. Acoust. Soc. Am., **68**(3), pp. 914–921.

[25] Guedra, M., Penelet, G., Lotton, P., and Dalmont, J., 2011, "Theoretical Prediction of the Onset of Thermoacoustic Instability From the Experimental Transfer Matrix of a Thermoacoustic Core," J. Acoust. Soc. Am., **130**(1), pp. 145–152.

[26] Giauque, A., Selle, L., Gicquel, L., Poinsot, T., Buechner, H., Kaufmann, P., and Krebs, W., 2005, "System Identification of a Large-Scale Swirled Partially Premixed Combustor Using LES and Measurements," J. Turbul., **6**, pp. 1–21.

[27] Tay-Wo-Chong, L., Bomberg, S., Ulhaq, A., Komarek, T., and Polifke, W., 2012, "Comparative Validation Study on Identification of Premixed Flame Transfer Function," ASME J. Eng. Gas Turbines Power, **134**(2), p. 021502.

[28] CERFACS and IMFT, 2008, "The AVBP HandBook," Cerfacs, Toulouse, France, accessed Oct. 10, 2017, http://www.cerfacs.fr/avbp6x/

[29] Nicoud, F., and Ducros, F., 1999, "Subgrid-Scale Stress Modelling Based on the Square of the Velocity Gradient Tensor," Flow Turbul. Combust., **62**(3), pp. 183–200.

[30] Colin, O., Ducros, F., Veynante, D., and Poinsot, T., 2000, "A Thickened Flame Model for Large Eddy Simulation of Turbulent Premixed Combustion," Phys. Fluids, **12**(7), pp. 1843–1863.

[31] Polifke, W., Wall, C., and Moin, P., 2006, "Partially Reflecting and Non-Reflecting Boundary Conditions for Simulation of Compressible Viscous Flow," J. Comput. Phys., **213**(1), pp. 437–449.

[32] Merk, M., Gaudron, R., Gatti, M., Mirat, C., Schuller, T., and Polifke, W., 2018, "Measurement and Simulation of Combustion Noise and Dynamics of a Confined Swirl Flame," AIAA J., **56**(5), pp. 1930–1942.

[33] Yang, Y., Noiray, N., Scarpato, A., Schulz, O., Düsing, K. M., and Bothien, M., 2015, "Numerical Analysis of the Dynamic Flame Response in Alstom Reheat Combustion Systems," ASME Paper No. GT2015-42622.

[34] Innocenti, A., Andreini, A., and Facchini, B., 2015, "Numerical Identification of a Premixed Flame Transfer Function and Stability Analysis of a Lean Burn Combustor," Energy Procedia, **82**, pp. 358–365.

[35] Kopitz, J., Bröcker, E., and Polifke, W., 2005, "Characteristics-Based Filter for Identification of Planar Acoustic Waves in Numerical Simulation of Turbulent Compressible Flow," 12th International Congress on Sound and Vibration (ICSV12), Lisbon, Portugal, July 11–14.

[36] Dowling, A. P., and Stow, S. R., 2003, "Acoustic Analysis of Gas Turbine Combustors," J. Propul. Power, **19**(5), pp. 751–764.

[37] Li, J., and Morgans, A. S., 2015, "Time Domain Simulations of Nonlinear Thermoacoustic Behaviour in a Simple Combustor Using a Wave-Based Approach," J. Sound Vib., **346**, pp. 345–360.

[38] Emmert, T., Jaensch, S., Sovardi, C., and Polifke, W., 2014, "TaX—A Flexible Tool for Low-Order Duct Acoustic Simulation in Time and Frequency Domain," 7th Forum Acusticum, Krakow, Poland, Sept., pp. 7–12.

[39] Bothien, M., Moeck, J., Lacarelle, A., and Paschereit, C. O., 2007, "Time Domain Modelling and Stability Analysis of Complex Thermoacoustic Systems," Proc. Inst. Mech. Eng., Part A, **221**(5), pp. 657–668.

[40] Lieuwen, T. C., 2012, *Unsteady Combustor Physics*, Cambridge University Press, New York.